

# Hydrophobic and antireflective characteristics of thermally oxidized periodic Si surface nanostructures

J.W. Leem · Y.M. Song · J.S. Yu

Received: 30 August 2011 / Revised version: 6 February 2012 / Published online: 20 April 2012  
© Springer-Verlag 2012

**Abstract** We reported the antireflective properties of periodic silicon (Si) subwavelength gratings and flat substrates in combination with thermal oxidation for an effective surface passivation. Moreover, theoretical calculations and analysis based on rigorous coupled-wave analysis simulation were performed. For thermally oxidized Si subwavelength grating structures, the reflectance was significantly reduced compared to that of the thermally oxidized flat Si substrates in wide ranges of wavelengths and angles of incidence. As the oxidation time increased, the reflectance became lower with increasing  $\text{SiO}_x$  thickness on Si subwavelength gratings due to the more graded effective refractive index profile from air to the Si via the thermally oxidized Si subwavelength gratings with increased height. By incorporating a thermal oxidation process into the Si subwavelength gratings, a more hydrophobic surface with good surface passivation was obtained.

## 1 Introduction

Silicon (Si) is a crucial material used in optical and optoelectronic devices such as image sensors, photodetectors, and solar cells [1–3]. For these applications, it is very important to enhance the light extraction or absorption efficiency in the

devices. Due to the high refractive index of Si, its surface typically exhibits a high reflectivity to incident light. For high-performance Si-based devices, therefore, antireflection coatings, which can suppress the unwanted surface reflection losses, have been employed. Recently, subwavelength gratings inspired from the moth eye effect have attracted a great deal of attention because they are more stable and durable than the conventional multilayer antireflection coatings which have some disadvantages of thermal mismatch, material selection, layer thickness control, and a limit of the low-reflectance band in wavelengths [4–7]. The periodic subwavelength gratings with a gradual change in effective refractive index between air and the semiconductor material make it easy to control the surface relief profile and to enhance the optical efficiency in wide ranges of wavelengths and angles of incidence [8]. However, to fabricate the subwavelength gratings with periodic patterns, a dry etching process is often required, which may induce defects at the semiconductor surface, thus resulting in the degradation of reliability and lifetime due to the increase of the carrier recombination at the surface [9].

In practical applications, the surface of subwavelength gratings should be electrically well passivated in order to keep the surface recombination losses, which occur largely via the defects at the surface, at tolerable levels. To overcome this problem, silicon dioxide ( $\text{SiO}_2$ ) thin films on the Si surface as a passivation layer as well as an antireflection coating layer have often been used [10, 11]. However, there has been very little work reported on the optical properties of thermally oxidized Si-based nanostructures (or subwavelength gratings). Meanwhile, a self-cleaning surface feature has been found to be very useful in removing any surface dirt or dust particles for device applications [12]. Additional surface modifications may be required to enhance the surface hydrophobicity. In this work, we investigated the an-

---

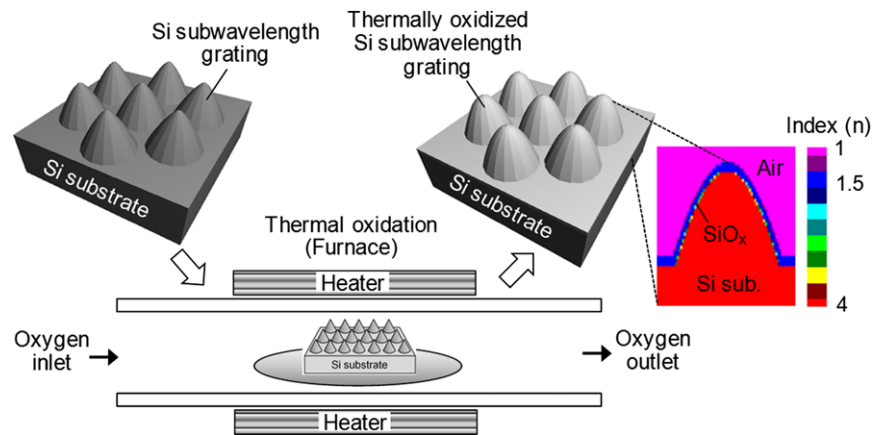
J.W. Leem · J.S. Yu (✉)

Department of Electronics and Radio Engineering, Institute for Laser Engineering, Kyung Hee University, 1 Seocheon-dong, Giheung-gu, Yongin-si, Gyeonggi-do 446-701, Republic of Korea  
e-mail: jsyu@khu.ac.kr  
Fax: +82-31-2062820

Y.M. Song

Department of Materials Science and Engineering, University of Illinois at Urbana-Champaign, Urbana, IL 61801, USA

**Fig. 1** Schematic diagram for the fabrication procedure of thermally oxidized Si subwavelength grating structures by using a furnace system. The refractive-index profile of the thermally oxidized Si subwavelength grating structures is also shown



antireflective properties of the thermally oxidized Si subwavelength grating structures with two-dimensional (2D) periodic closely packed patterns, together with theoretical calculations using the rigorous coupled-wave analysis (RCWA) simulation. The wetting behavior of water droplets and the electrical passivation property were also studied.

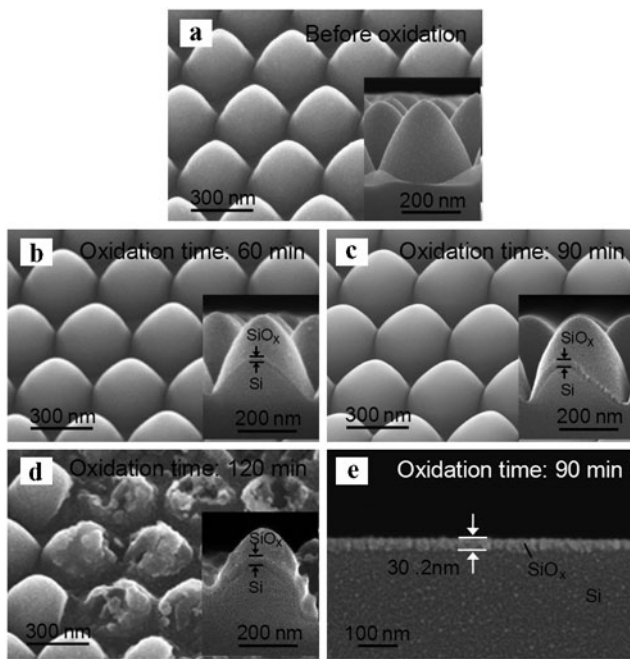
## 2 Experimental details

Figure 1 shows the schematic diagram for the fabrication procedure of thermally oxidized Si subwavelength grating structures by using a furnace system. The refractive-index profile of the thermally oxidized Si subwavelength grating structures is also shown. For the fabrication of conical Si subwavelength gratings with a 2D periodic structure, p-type (100) Si substrates with a size of  $2 \times 2 \text{ cm}^2$  were used. The substrate thickness and resistivity were  $\sim 525 \text{ }\mu\text{m}$  and  $\sim 3.5 \text{ }\Omega \text{ cm}$ , respectively. The period and height of the fabricated Si subwavelength gratings were about 300 nm and 280 nm, respectively. The details of the fabrication method were described in our previous work [13]. After the Radio Corporation of America (RCA) standard cleaning, the thermal oxidation process of the Si subwavelength gratings and flat Si substrates was carried out at the temperature of 1000 °C for the surface passivation. The process pressure and oxygen flow rate were kept at 50 Torr and 200 sccm, respectively. To investigate the effect of the thickness of oxidized Si (i.e. SiO<sub>x</sub>) on the antireflective property of the thermally oxidized Si subwavelength grating structures, the thermal oxidation time was varied from 60 to 120 min. The SiO<sub>x</sub> layer on the Si subwavelength gratings was formed by an oxygen diffusion process into the Si. As shown in the index profile of Fig. 1, the effective refractive index in the thermally oxidized Si subwavelength grating structures is gradually changed from  $n_{\text{air}} = 1$  to  $n_{\text{Si}} \sim 4$  (i.e. at a wavelength of 550 nm) via  $n_{\text{SiO}_x} \sim 1.5$ . The structural morphology and

layer thickness of the fabricated thermally oxidized Si subwavelength gratings and flat substrates were observed by using a scanning electron microscope (SEM, Carl Zeiss, LEO SUPRA 55). The optical reflectance was measured by an UV–vis–NIR spectrophotometer (Varian, Cary 5000) using linearly polarized incident light at an angle of near-normal incidence (i.e.  $\sim 8^\circ$ ). The water contact angles were measured by using a contact angle measurement system (SEO Co. Ltd., Phoenix-300). The effective electrical properties of the samples were measured by using a Hall effect measurement system (Accent, HL5500PC) with a magnetic field of 0.32 T at room temperature. For this, indium contacts were deposited onto the corners of square-shaped samples with a size of  $1 \times 1 \text{ cm}^2$  in the van der Pauw geometry [14]. Then, the samples were heated on a hot plate at the temperature of 180 °C for 3 min.

## 3 Results and discussion

Figure 2 shows the SEM images of (a) the Si subwavelength grating and the thermally oxidized Si subwavelength gratings at oxidation times of (b) 60 min, (c) 90 min, and (d) 120 min. The insets show the cross-sectional SEM images of the corresponding structures. The shape of the subwavelength gratings relies on the oxidation time. As shown in Fig. 2a, the 2D periodic subwavelength grating with a six-fold hexagonal cone-shaped structure was formed on the Si substrate. It can be observed that the SiO<sub>x</sub> thin films were well covered on the Si subwavelength gratings by both internal and superficial oxidation reactions through the thermal oxidation process. When the Si is thermally oxidized, the oxide area is formed with a ratio of approximately 46 % for the internal oxidation and 54 % for the superficial oxidation at the surface of the original Si substrate [15, 16]. Thus, the overall volume of the thermally oxidized Si subwavelength gratings was also extended with increasing oxidation time. As the oxidation time was increased to 90 min, the



**Fig. 2** SEM images of (a) the Si subwavelength grating and the thermally oxidized Si subwavelength gratings at oxidation times of (b) 60 min, (c) 90 min, and (d) 120 min. The insets show the cross-sectional SEM images of the corresponding structures. The cross-sectional SEM image of the thermally oxidized flat Si substrate at 90 min is also shown in (e)

shape of the thermally oxidized Si subwavelength gratings became more parabolic with an extended volume compared to the Si subwavelength grating before the thermal oxidation. At 120 min, however, the subwavelength gratings were apparently distorted and collapsed, as can be seen in Fig. 2d. During the thermal oxidation process, volume expansion occurs perpendicular to the local Si surface [17]. The excess oxidation time may cause additional stresses on the Si, especially in the submicron structures [18]. The  $\text{SiO}_x$  thickness of the thermally oxidized Si subwavelength gratings was gradually increased from  $\sim 20 \pm 1.4$  nm at 60 min to  $\sim 39 \pm 2.2$  nm at 120 min with increasing oxidation time. The cross-sectional SEM image of the thermally oxidized flat Si substrate at 90 min is also shown in Fig. 2e. Similarly, the  $\text{SiO}_x$  layer with a thickness of  $\sim 30.2 \pm 2$  nm was well formed on the surface of the flat Si substrate by the thermal oxidation process.

Figure 3a shows the measured reflectance spectra of the flat Si substrate, the Si subwavelength grating, and the thermally oxidized flat Si substrates and thermally oxidized Si subwavelength gratings at different oxidation times. The Si subwavelength grating (black solid curve) effectively suppressed the surface reflection compared to the flat Si substrate (pink solid curve), indicating the reflectance of  $< 17.6\%$  in the wavelength region of 300–2100 nm due to the gradient effective refractive index between the Si and air. Clearly, the reflectance was further reduced over a wide

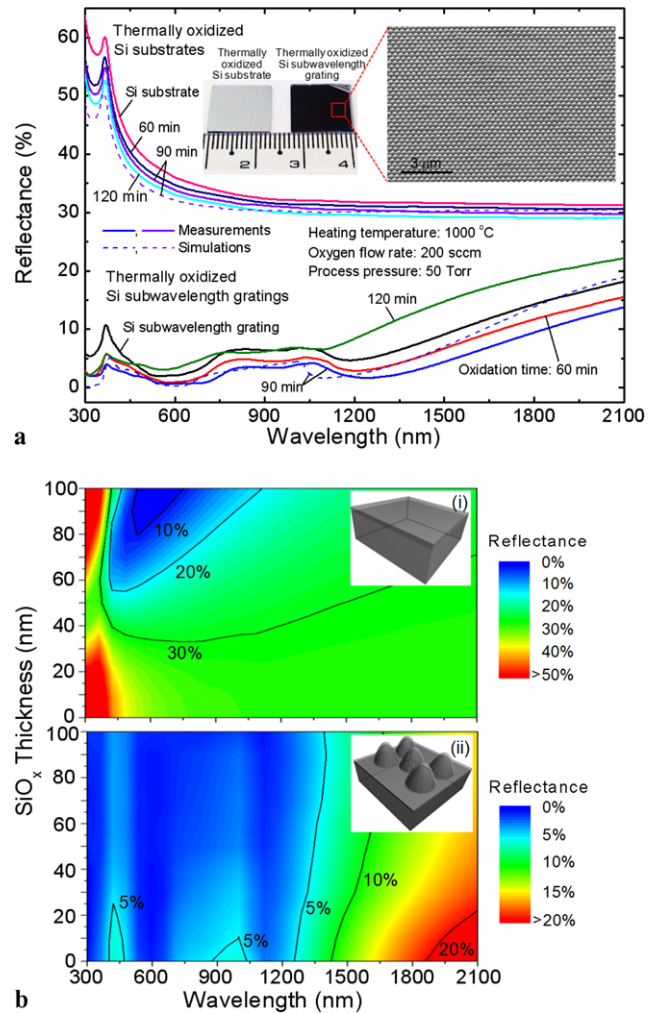


**Fig. 3** (a) Measured reflectance spectra (solid curves) of the flat Si substrate, the Si subwavelength grating, and the thermally oxidized flat Si substrates and thermally oxidized Si subwavelength gratings at different oxidation times and (b) contour plots of the variation of calculated reflectance as a function of the  $\text{SiO}_x$  thickness of (i) the thermally oxidized flat Si substrate and (ii) the thermally oxidized Si subwavelength grating with a period of 300 nm at wavelengths of 300–2100 nm. The calculated reflectance spectra of the thermally oxidized Si subwavelength grating (blue dashed curve) and the thermally oxidized flat Si substrate (violet dashed curve) with a 30-nm-thick  $\text{SiO}_x$  layer are also shown in (a). The insets of (a) show the photographs (left) of the fabricated thermally oxidized flat Si substrate and the thermally oxidized Si subwavelength grating samples at 90 min and the zoomed-out SEM image (right) of the thermally oxidized Si subwavelength grating at 90 min. The insets of (i) and (ii) in (b) show the 3D models of the thermally oxidized flat Si substrate and the thermally oxidized Si subwavelength grating used in this simulation, respectively

wavelength region of 300–2100 nm when the Si subwavelength gratings were thermally oxidized for 60 min (red solid curve) and 90 min (blue solid curve). This can be attributed to the more graded refractive-index profile, resulting from the fact that the subwavelength gratings are changed into a more parabolic shape with their increased height as the  $\text{SiO}_x$  thickness is increased. Similarly, this re-

duction was observed in the reflectance spectra of the thermally oxidized flat Si substrates, as shown in Fig. 3a. Particularly, for the thermally oxidized Si subwavelength grating at 90 min (blue solid curve), the reflectance was lower than 13.7 % at wavelengths of 300–2100 nm, indicating an average reflectance of  $\sim 4.75$  %. However, although the thickness of  $\text{SiO}_x$  was greater at 120 min, the reflectance spectrum (green solid curve) was considerably increased (i.e. especially in the wavelength range longer than  $\sim 1100$  nm) due to the scattering caused by the distortion in the Si subwavelength gratings, as shown in Fig. 2d. For comparison, the calculated reflectance spectra of the thermally oxidized Si subwavelength grating (blue dashed curve) and the thermally oxidized flat Si substrate (violet dashed curve) with a 30-nm-thick  $\text{SiO}_x$  layer are also shown in Fig. 3a. The calculated reflectance spectra (i.e. blue and violet dashed curves) exhibit a reasonable agreement with the measured reflectance data of the thermally oxidized Si subwavelength grating (blue solid curve) and flat Si substrate (violet solid curve) at 90 min though both results are not matched perfectly, due to the difficulty in matching exactly the geometric simulation model to the actual fabricated structure as well as the refractive-index mismatch of the Si and  $\text{SiO}_x$  used in this calculation and experiment. The photographs (left) of the fabricated thermally oxidized flat Si substrate and thermally oxidized Si subwavelength grating samples and the zoomed-out SEM image (right) of the thermally oxidized Si subwavelength grating at 90 min are shown in the insets of Fig. 3a. The thermally oxidized Si subwavelength grating sample has a dark black surface compared to the thermally oxidized flat Si substrate, indicating a very low surface reflectivity as confirmed in Fig. 3a. It can be observed that the fabricated thermally oxidized Si subwavelength grating structure is very uniform and closely packed over a large area.

For theoretical analysis, the reflection properties of the thermally oxidized Si subwavelength gratings were simulated using the RCWA method [19]. Figure 3b shows the contour plots of the variation of the calculated reflectance as a function of the  $\text{SiO}_x$  thickness of (i) the thermally oxidized flat Si substrate and (ii) the thermally oxidized Si subwavelength grating with a period of 300 nm at wavelengths of 300–2100 nm. The insets of (i) and (ii) in Fig. 3b show the three-dimensional (3D) models of the thermally oxidized flat Si substrate and the thermally oxidized Si subwavelength grating used in this simulation, respectively. For the simulation models, the periodic geometry of the thermally oxidized Si subwavelength grating was obtained from our previous work [20]. In simulations, the height, the bottom radius, and the order of taper of the Si subwavelength gratings were assumed to be 280 nm, 120 nm, and 1, respectively. The thickness of the Si substrate was fixed at 525  $\mu\text{m}$ . To obtain more precisely calculated results, we assumed that

the  $\text{SiO}_x$  layer of the thermally oxidized Si subwavelength grating and the thermally oxidized flat Si substrate was set at a ratio of 46 % below and 54 % above the original surface of each structure when the  $\text{SiO}_x$  thickness was increased, as mentioned above. In this case, the height and thickness of the Si in the subwavelength grating and flat substrate were slightly reduced with the ratio of 46 % of the  $\text{SiO}_x$  thickness. The order of taper of the Si subwavelength grating was assumed to be also increased by 0.1 when the  $\text{SiO}_x$  thickness was increased by a step of 10 nm. The reflectance is decreased as the  $\text{SiO}_x$  thickness of the thermally oxidized Si subwavelength grating is increased, which exhibits a similar trend to the measured data in Fig. 3a. This is the reason that the height of the thermally oxidized Si subwavelength gratings is not only increased, but also the effective refractive index from the Si to air via the  $\text{SiO}_x$  in the Si subwavelength gratings is more linearly changed like the parabola-shaped structure [8, 21–23]. For  $\text{SiO}_x$  thicknesses above 30 nm, the calculated reflectance spectra of the thermally oxidized Si subwavelength grating exhibit values lower than 19.1 % over a wide wavelength range of 300–2100 nm, indicating the low reflection region of  $< 10$  % at wavelengths below  $\sim 1550$  nm. For the thermally oxidized flat Si substrate, on the other hand, a low reflection band below 10 %, which is exhibited as a blue part, is formed at  $\text{SiO}_x$  thicknesses above 80 nm in the wavelength region of 500–750 nm, as shown in (i) of Fig. 3b. From the simulation results, we noted that the low-reflection band is shifted by varying the  $\text{SiO}_x$  thickness on the flat Si surface, while it is not much changed on the Si subwavelength grating surface.

The incident angle-dependent antireflection properties of the thermally oxidized Si subwavelength grating structures were also explored using a Cary variable angle specular reflectance accessory in the specular mode, by changing the angle ( $\theta_i$ ) of incident light from 8 to 70°. Figure 4a shows the measured incident angle-dependent reflectance spectra of the thermally oxidized Si subwavelength grating structure at the oxidation time of 90 min. As the angle of incidence was increased from  $\theta_i = 20^\circ$  (violet solid curve) to  $50^\circ$  (pink solid curve), the average reflectance value was not much increased from 5.42 to 8.65 % in the wavelength region of 300–2100 nm, maintaining the reflectance spectra below  $\sim 13$  %. On the contrary, for angles of incidence more than  $\theta_i = 60^\circ$  (navy and red solid curves), it can be observed that the reflectance was noticeably increased. However, the reflectance spectrum was still low (i.e.  $< \sim 28$  %) compared to that of the thermally oxidized flat Si substrate (Fig. 3a) at the angle of normal incidence in spite of the high incident angle of  $\theta_i = 70^\circ$  (red solid curve), which exhibited an average reflectance of  $\sim 19.5$  %. For comparison, the contour plot of calculated incident angle-dependent reflectance spectra of the thermally oxidized Si subwavelength grating with the  $\text{SiO}_x$  thickness of 30 nm is also shown in



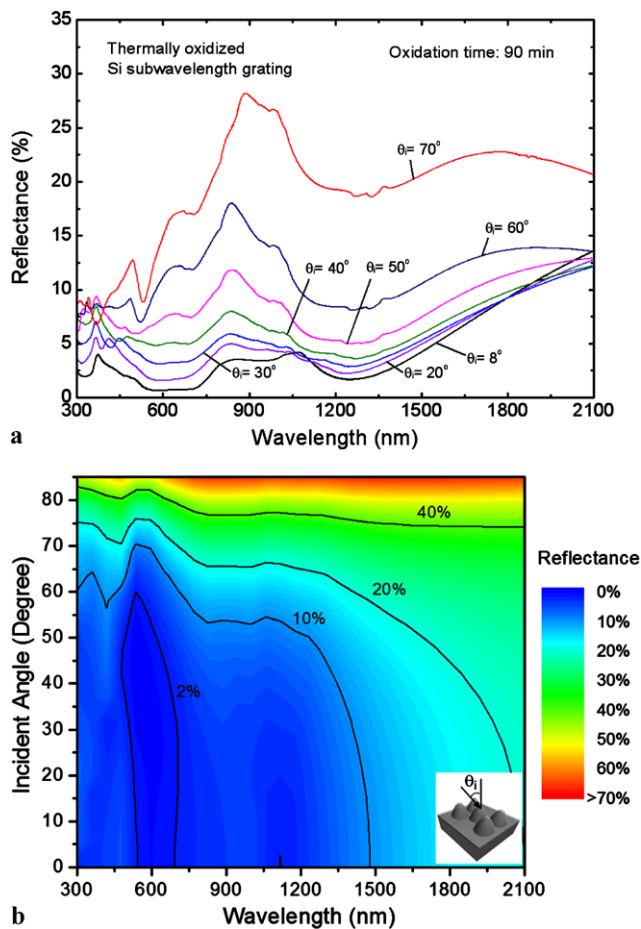


**Fig. 4** (a) Measured incident angle-dependent reflectance spectra of the thermally oxidized Si subwavelength grating at the oxidation time of 90 min and (b) contour plot of the variation of reflectance as functions of angle of incidence and wavelength for the thermally oxidized Si subwavelength grating with the  $\text{SiO}_x$  thickness of 30 nm

Fig. 4b. The inset shows the 3D simulation model used in (ii) of Fig. 3b. The calculated reflectance was not much dependent on the angle of incidence up to  $\theta_i = 50^\circ$  and then it rapidly increased. Although there are some differences between the experimentally measured and theoretically calculated results, they roughly give a similar tendency in wide ranges of wavelengths and angles of incidence.

Figure 5 shows the photographs of water droplets on the surfaces of (a) the Si substrate, (b) the Si subwavelength grating before the thermal oxidation, (c) the thermally oxidized Si substrate, and (d) the thermally oxidized Si subwavelength grating structure. The oxidation time was 90 min. The water contact angles were estimated by averaging the measured data at three different positions on the surface of the samples. Generally, the Si subwavelength grating structure exhibits hydrophobicity while the flat Si substrate has a hydrophilic property. It was found that the water contact angle of the thermally oxidized Si subwavelength grating was larger than that of the Si subwavelength grating

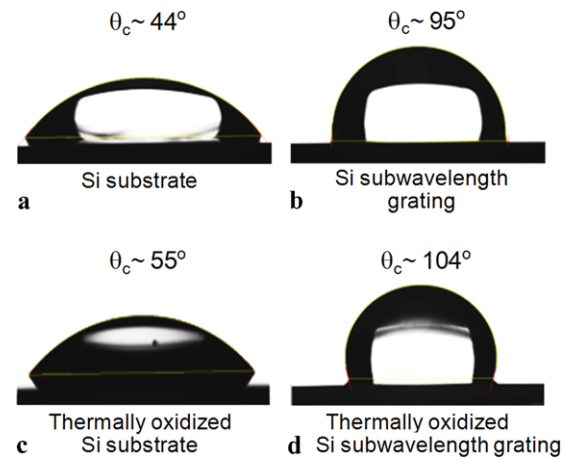


**Fig. 5** Photographs of water droplets on the surfaces of (a) the Si substrate, (b) the Si subwavelength grating before thermal oxidation, (c) the thermally oxidized Si substrate, and (d) the thermally oxidized Si subwavelength grating structure. The oxidation time was 90 min

before thermal oxidation. This results from the nanosized structure and thin  $\text{SiO}_x$  layer in the thermally oxidized Si subwavelength grating [12, 24, 25]. For the thermally oxidized Si subwavelength grating, its contact angle ( $\theta_c$ ) was about  $104^\circ$ , which is larger than  $\theta_c \sim 55^\circ$  of the thermally oxidized Si substrate and  $\theta_c \sim 95^\circ$  of the Si subwavelength grating before thermal oxidation, indicating a hydrophobic surface.

In order to investigate the passivation effect of the  $\text{SiO}_x$  thin film on the effective electrical properties (i.e. resistivity, carrier concentration, and Hall mobility) of the thermally oxidized Si subwavelength grating structure, we performed Hall effect measurements. For the thermally oxidized Si subwavelength grating at 90 min, the effective resistivity of  $237.1 \, \Omega \text{ cm}$  was higher than  $12.6 \, \Omega \text{ cm}$  of the Si subwavelength grating before thermal oxidation, indicating the Hall mobility and carrier concentration of  $296 \, \text{cm}^2 \text{ V}^{-1} \text{ s}^{-1}$  and  $4.63 \times 10^{12} \, \text{cm}^{-3}$  (i.e.  $350 \, \text{cm}^2 \text{ V}^{-1} \text{ s}^{-1}$  and  $7.35 \times 10^{13} \, \text{cm}^{-3}$  for the Si subwavelength grating), respectively. This may be attributed to the decrease in the Hall mobility and carrier concentration of the thermally oxidized Si subwavelength grating compared to the Si subwavelength grating due to the formation of  $\text{SiO}_x$  as a passivation layer on the Si subwavelength grating by the oxygen diffusion process into the Si. Therefore, the thermal oxidation of the Si subwavelength grating can be used to further enhance its self-cleaning property as well as to provide a good electrical surface passivation.

#### 4 Conclusion

We experimentally and theoretically investigated the antireflective properties of thermally oxidized Si subwavelength

gratings by the thermal oxidation process for electrically passivating the Si surface. The measured data and calculated results showed a reasonably similar tendency. The thermally oxidized Si subwavelength gratings with a hydrophobic surface exhibited much lower reflectance compared to the thermally oxidized flat Si substrates over the wide ranges of wavelengths of 300–2100 nm and incident angles of 8–70° for different thicknesses of SiO<sub>x</sub> on the subwavelength gratings. At 90 min of oxidation time, the effective resistivity of the thermally oxidized Si subwavelength gratings was increased compared to the Si subwavelength gratings before thermal oxidation, leading to a good electrical surface passivation. These results suggest that the broadband and omnidirectional antireflective thermally oxidized periodic Si subwavelength grating structures with a hydrophobic and electrically passivated surface are a potential candidate for Si-based optical and optoelectronic devices.

**Acknowledgement** This research was supported by the Basic Science Research Program through the NRF funded by the MEST (Nos. 2011-0003857 and 2011-0026393).

## References

1. K. Rosan, IEEE Trans. Electron Devices **36**, 2923 (1989)
2. M.A. Green, J. Zhao, A. Wang, P.J. Reece, M. Gal, Nature **412**, 805 (2001)
3. J. Zhao, Sol. Energy Mater. Sol. Cells **82**, 53 (2004)
4. M.Y. Chiu, C.H. Chang, M.A. Tsai, F.Y. Chang, P. Yu, Opt. Express **18**, A308 (2010)
5. Y.M. Song, H.J. Choi, J.S. Yu, Y.T. Lee, Opt. Express **18**, 13063 (2010)
6. J.W. Leem, Y.M. Song, Y.T. Lee, J.S. Yu, Appl. Phys. B **99**, 695 (2010)
7. B.J. Kim, J. Kim, Opt. Express **19**, A326 (2011)
8. D.G. Stavenga, S. Foletti, G. Palasantzas, K. Arikawa, Proc. R. Soc. Lond. B, Biol. Sci. **273**, 661 (2006)
9. G. Kumaravelu, M.M. Alkaisi, A. Bittar, D. Macdonald, J. Zhao, Curr. Appl. Phys. **4**, 108 (2004)
10. L. Debarge, J.P. Stoquert, A. Slaoui, L. Stalmans, J. Poortmans, Mater. Sci. Semicond. Process. **1**, 281 (1998)
11. A.G. Aberle, Prog. Photovolt. Res. Appl. **8**, 473 (2000)
12. J. Zhu, C.M. Hsu, Z. Yu, S. Fan, Y. Cui, Nano Lett. **10**, 1979 (2010)
13. J.W. Leem, Y.M. Song, Y.T. Lee, J.S. Yu, Appl. Phys. B **100**, 891 (2010)
14. L.J. van der Pauw, Philips Res. Rep. **13**, 1 (1958)
15. C. Zhang, K. Najafi, J. Micromech. Microeng. **14**, 769 (2004)
16. J. Park, L.H. Chen, D. Hong, C. Choi, M. Loya, K. Brammer, P. Bandaru, S. Jin, Nanotechnology **20**, 015303 (2009)
17. P.J. Cousins, J.E. Cotter, Sol. Energy Mater. Sol. Cells **90**, 228 (2006)
18. S.M. Hu, J. Appl. Phys. **70**, R53 (1991)
19. M.G. Moharam, Proc. SPIE **883**, 8 (1988)
20. Y.H. Ko, J.S. Yu, Opt. Express **19**, 297 (2011)
21. Y.M. Song, S.J. Jang, J.S. Yu, Y.T. Lee, Small **6**, 984 (2010)
22. K. Choi, S.H. Park, Y.M. Song, Y.T. Lee, C.K. Hwangbo, H. Yang, H.S. Lee, Adv. Mater. **22**, 3713 (2010)
23. J.W. Leem, D.H. Joo, J.S. Yu, Sol. Energy Mater. Sol. Cells **95**, 2221 (2011)
24. Y. Sato, M. Maeda, Jpn. J. Appl. Phys. **33**, 6508 (1994)
25. K. Matsushita, T. Monbara, K. Nakayama, H. Nagamura, S. Okuyama, K. Okuyama, Electron. Commun. Jpn., Part 2, Electron. **84**, 51 (2001)